

# Development of a D-band Traveling Wave Tube for high data rate wireless links

Rupa Basu, *Student, IEEE*, Jeevan M. Rao *Student, IEEE*, Trung Le, Rosa Letizia *Senior Member, IEEE*, and Claudio Paoloni *Senior Member, IEEE*

**Abstract**—Ubiquitous wireless distribution of multi-gigabit per second data rate for enabling new 5G and 6G paradigms can be only achieved by exploiting the wide frequency bands available in the sub-THz spectrum (90 - 305 GHz). The high total attenuation at sub-THz, in particular due to rain and humidity, poses a substantial challenge to achieve long links, not yet resolved due to the lack of sources with adequate transmission power. Sub-THz traveling wave tubes are emerging as key components to ensure high signal to noise ratio over a large coverage area or for long distance. This paper will describe the design and fabrication of a novel TWT for enabling point to multipoint wireless distribution at D-band (141 - 148.5 GHz). To be suitable for the wireless market, TWTs need to be low cost and of easy manufacture for large scale production. The proposed D-band TWT uses a double corrugated waveguide as slow wave structure and a new electron gun, both designed for easy assembly and low fabrication cost. The paper describes the design process, the development of the parts of the TWT and the first prototype assembly.

**Index Terms**—TWT, D-band, double corrugated waveguide, millimeter waves, sub-THz

## I. INTRODUCTION

**F**UTURE wireless networks are expected to support enormous data traffic predicted in the new 5G and 6G concepts. The wide frequency bands at sub-THz frequencies, namely, W-band (92 - 110 GHz), D-band (141 - 174.8 GHz) and G-band (210-310 GHz), offer the support of tens or hundreds of gigabit per second data rate precluded to the sub - 6 GHz range and the low millimeter wave frequencies (up to 90 GHz) [1].

Point to point (PtP) links at D-band have been demonstrated, but limited to less than a few hundreds meter range due to the high total attenuation given by free space path loss, humidity and rain, not compensated by adequate transmission power due to the limitations of solid state power amplifiers (SSPAs). As a result, those links are affected by low signal to noise ratio (SNR) or short link range. That prevents the use of high modulation schemes or requires the use very high gain high

The work has received funding from the European Commission Horizon 2020 research and innovation programs under grant agreement no 762119. This work reflects only the author view and the Commission is not responsible of any use that may be made of the information it contains

Rupa Basu, Jeevan M. Rao, Rosa Letizia and Claudio Paoloni, are with Engineering Department, Lancaster University, Lancaster, LA1 4YW UK (e-mail: c.paoloni@lancaster.ac.uk). Trung Lee is with Hubner GmbH, Germany

directivity antennas. In addition, point to point distribution is not convenient to feed the planned deployment of dense small cells due to the footprint of the numerous front ends needed, difficulty of installation and complex network parameters.

Point to multipoint (PmP) distribution is the actual modality for mobile networks at sub-6 GHz. It has substantial advantages in comparison to PtP, such as no need of frequency planning, lower Total Cost of Ownership (TCO), easy and flexible installation. At sub-THz frequency, PmP would be the ideal solution for feeding high density small cell deployment [2]. A PmP front end uses a low gain antenna with wide beam angle. Therefore, at sub-THz frequencies, for the same range of an equivalent PtP system a higher transmission power is needed, not available by SSPAs, preventing the PmP distribution.

Traveling wave tubes (TWTs) have been demonstrated to provide up to tens of Watt in the sub-THz spectrum, depending on the operation frequency [1], [3], [4], more than one order of magnitude higher than SSPAs at the same frequency. This transmission power is sufficient to satisfy link budgets for sub-THz PmP and enabling long range with high SNR.

The European Commission Horizon 2020 project TWEET-HER realized and tested the first ever point to multipoint links at W-band (92 - 95 GHz). The enabling device is a TWT with 40 W output power and about 40 dB gain [4].

A second Horizon 2020 project, ULTRAWAVE [5] is in the final stage of development for the realisation of the first ever point to multipoint wireless network at D-band (141 - 148.5 GHz) with transport at G-band (275 - 305 GHz) between PmP sectors [6], [7] enabled by novel TWTs. The PmP transmission hub needs a saturated power of about 10 W to satisfy the link budget for an area sector of 30° and 600 m radius, defined in the network architecture. To note that SSPAs (e.g. InP process) provide no more than one or two hundreds mW maximum.

One of the main requirements for TWTs to be introduced in the wireless communication market is low cost and ease of manufacturing for the large scale production.

The design and fabrication of sub-THz TWTs is a long and challenging process [8] due to the small dimensions, fabrication difficulties, possible failure of intermediate steps in part fabrication. Presently, only a few D-band TWT are reported in literature based on the folded waveguide [3], [9], [10], [11].

In this paper, the challenges and the solutions for the design and fabrication of a novel D-band TWT (141 - 148.5 GHz)

to enable the first Point to multipoint wireless distribution at D-band will be discussed. The TWT is realized by using a double corrugated waveguide slow wave structure and a novel configuration of electron gun of simple assembly, for low cost fabrication. Section II reports the design and simulations of the parts of the D-band TWT. Section III reports the fabrication of the parts and some measurements.

## II. D-BAND TWT DESIGN

D-band traveling wave tubes for the wide wireless market have to be affordable, easy to fabrication and assemble, with long lifetime. The most critical parts are the slow wave structure (SWS), whose dimensions are dictated by the short wavelength at 140 GHz, and the electron gun. At sub-THz frequency, SWSs suffer from low interaction impedance in comparison to the helix and high metal losses. The low interaction impedance reduces the energy transferred from the electron beam to the RF signal and the high losses make slower the interaction process. Another important design parameter is the shape of the electron beam. Pierce electron guns are a well established technology for producing cylindrical beam, focussed by a conventional ppm (periodic permanent magnetic) system. The folded waveguide (FWG) has been already used in D-band TWTs with cylindrical electron beam [9], [10]. However, the FWG is difficult to fabricate at the increase of frequency and needs a high precision alignment of the two halves to avoid reflection resonances in band [12].

The double corrugated waveguide (DCW) has interaction impedance comparable with a folded waveguide, but is much easier to fabricate. It can be fabricated in two parts [13]. The full structure including the two rows of pillars, the waveguide and the couplers is fabricated in one part. A flat lid to close the circuit is the second part, removing the need of high alignment accuracy, with reduction of fabrication costs. The beam voltage can be kept below 13 kV.

The specification of the D-band TWT for PmP wireless distribution are listed in Table I.

### A. Double Corrugated Waveguide cold parameters

The double corrugated waveguide has been designed in the band 141 - 148.5 GHz, assuming an electron beam voltage of about 12.7 kV. One of the most important design parameters is the interaction impedance that at the increase of the frequency tends to reduce, limiting the TWT performance. The interaction impedance of the DCW mainly depends on the distance between the two rows of pillars ( $g$ ) and the cross section of the pillars. A specific study was performed on the shape of the pillars to increase the interaction impedance [14]. The triangular shape has been found to almost double the interaction impedance in comparison to the square shape. In the following, triangular section pillars will be considered. The geometry of the DCW is shown in Fig 1. The dimensions are listed in Table II. Fig. 1 shows the 3D model of the single cell with the triangular pillars. Particular attention has been devoted to define the dimensions to reduce the difficulty of CNC milling due to the small features.

TABLE I  
D-BAND TWT SPECIFICATIONS

Frequency	141 - 148.5 GHz
Output power	about 10 W
Gain	35 - 40 dB
Beam Voltage	12 - 13 kV
Beam current	50 - 60 mA
Collector	Single stage
Cooling	Forced air cooling with radiators
Input/ Output Port	WR 05

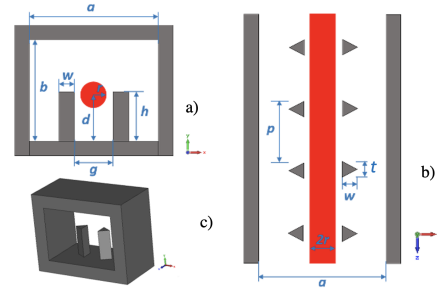


Fig. 1. Schematic of double corrugated waveguide with triangular pillars

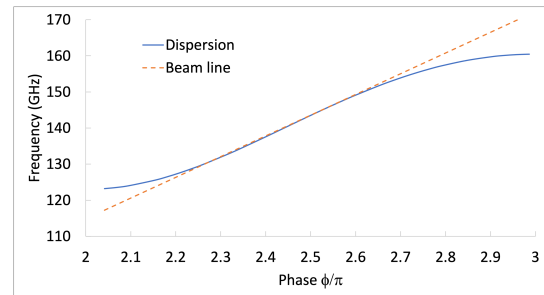


Fig. 2. Dispersion curve with 12.7 kV beam line superimposed

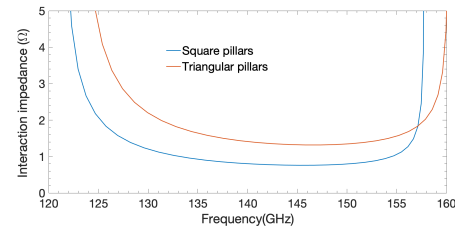


Fig. 3. Interaction impedance for triangular and rectangular pillar DCW

Fig.2 shows the dispersion curve with the superimposed 12.7 kV beam line, demonstrating a wide region of synchronism. The interaction impedance has been computed for two DCWs with same dimensions, one with square pillars and one with triangular pillars. It is notable the improvement obtained by using triangular pillars. The interaction impedance is about 1.5  $\Omega$ . The shape of the pillars has a minimum effect on the dispersion curve. All the simulations were performed by CST Microwave Studio [15].

### B. DCW design for large signal performance

The DCW needs a coupler to convert the propagating hybrid mode to the TE<sub>10</sub> mode at the flanges (WR05 in the considered frequency band). An effective coupling is realised by tapering

TABLE II  
DCW DIMENSIONS

Parameter	Dimension ( $\mu\text{m}$ )
Width (a)	875
Height (b)	648
Period (p)	575
Beam tunnel (g)	220
Pillar height (h)	350
Pillar width (w)	130
Pillar length (t)	130
Beam center (d)	200

the height of a specific number of pillars at both the ends of the DCW from the nominal value to zero. To note that the tapering reduces substantially the interaction impedance of the region where it is applied. To permit the beam flowing only in the interaction region of the DCW and reduce the overall TWT length, the DCW is bent  $90^\circ$  in correspondence of the input and output ports and the couplers are added after the bend. [16]. The couplers use square pillars that are easier to fabricate, since their lower interaction impedance is not relevant, not being part of the interaction section of the circuit. To verify the quality of the couplers a test structure with 20 periods, the input and the output couplers was simulated. A reduced copper conductivity  $\sigma = 2.89 \times 10^7$  S/m is assumed to model the contribution of losses of the metal surfaces due to a predicted surface roughness of about 100 nm. Figure 4 shows the S-parameters.  $S_{11}$  better than -15 dB is obtained over the operation band. The 20 periods test DCW simulated in (Fig. 4) was build (Fig. 5 left) to experimentally verify the transmission losses simulated with the reduced copper conductivity. The test DCW was fabricated in OFHC (Oxygen Free High Conductivity) copper by using a high precision CNC milling Primacon. The measurement shows lower losses than the simulation (Fig. 5 right), reassuring on quality of the fabrication and on the use of a correct conductivity value in the simulation.

To achieve 35 - 40 dB gain as in the specifications, two sections of DCW are adopted, separated by a sever to avoid oscillations (Fig. 6). A first performance evaluation was obtained by a single section DCW circuit to define the number of periods to achieve around 18 - 20 dB gain. Then a second section was designed to satisfy the final gain requirements. Extensive Particle in Cell (PIC) simulations (CST Particle Studio) were performed to optimize the number of periods of the two sections for output power and gain. The first section (DCW Short) was finally designed with 60 periods to provide about 18 dB gain sufficient to well modulate the beam. The second section (DCW Long) was designed with 110 periods to provide the required gain increase to get about 35 dB total gain. The  $S_{11}$  and  $S_{21}$  of the 60 and 110 period sections are shown in Fig. 4. To note the increase of losses at the increase of the number of periods.

The same parameters of the electron gun in Section C (12.7 kV beam voltage, 50 mA current and 160  $\mu\text{m}$  beam diameter) and a reduced copper conductivity ( $\sigma = 2.89 \times 10^7$  S/m) are used.

The gain and the output power of the two-section DCW are shown in Fig. 7 and in Fig. 8 respectively. It is notable

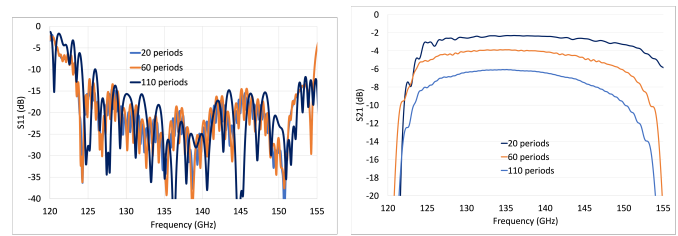


Fig. 4. S-parameters of the double corrugated waveguide 20 periods test circuit (the S-parameters with 60 and 110 periods are also included related to the DCW in Figure 6)

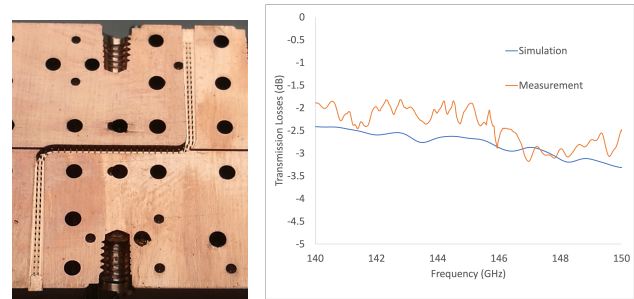


Fig. 5. Fabricated 20 period DCW (left) and transmission losses comparison simulated and measured values (right).

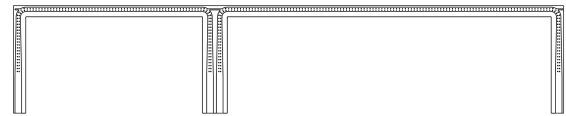


Fig. 6. Two section D-band TWT simulation domain

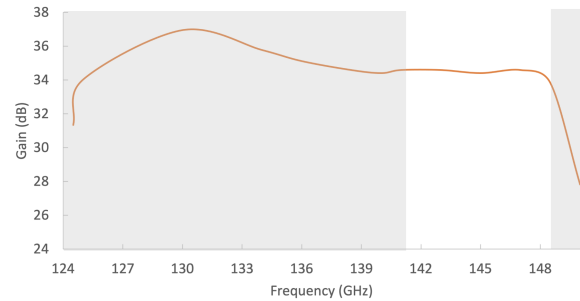


Fig. 7. Gain (white region is the 141 - 148.5 GHz operation band)

the useful frequency band much wider than the required band. A gain of about 35 dB, the output power better than 10 W, with 4 mW input power, and the low ripple in band, fully satisfy the design requirements. The inset in Fig. 8 shows the electron energy distribution along the z-axis. The Pin-Pout curve computed at 145 GHz shows a good linearity below 3 dBm. This is particularly important for wireless links, since the TWT has to work in high linearity region with 6 dB or more back-off below saturation. To note the 4 mW (6 dBm) input power (used in Fig. 8) is close to the 1dB compression point. At full saturation the output power is about 16 W.

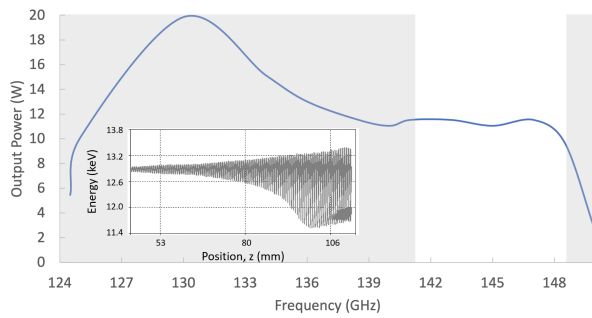


Fig. 8. Output power with 4 mW input power (white region is the 141 - 148.5 GHz operation band) (inset: electron energy)

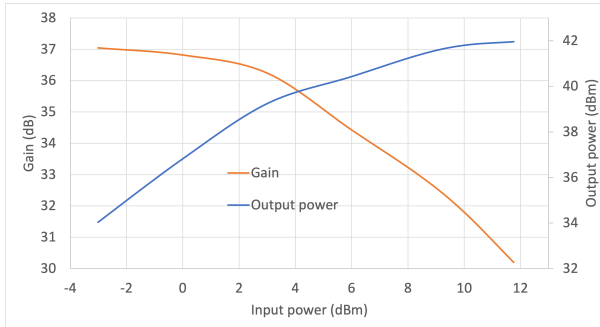


Fig. 9. Pin-Pout and gain curves computed at 145 GHz

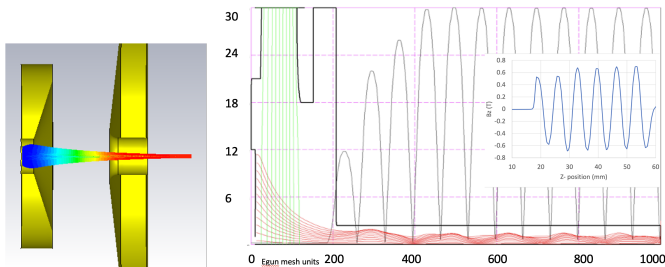


Fig. 10. Beam optics simulation (left) and Magnetic focussed beam (right) with magnetic field intensity and distribution (inset)

### C. Electron optics design

The electron optics was simulated by both CST Particle Tracking Solver and EGUN. The design parameters for the electron optics are 12 kV beam voltage, 56 mA current and 160  $\mu\text{m}$  beam diameter. A cathode with 1.2 mm diameter and 10 mm spherical radius is used. The anode is placed at 4.9 mm from the cathode. The 3D simulation performed by CST is shown in Fig 10 (right). The same behaviour was confirmed by EGUN simulations.

### D. Magnetic focussing

A permanent periodic magnetic (ppm) focussing is used. The magnetic field is set at 0.6 T. It consists of a stack of Samarium Cobalt magnets assembled with iron pole pieces. The simulation by EGUN of the electron beam confined by the ppm system shows a very good focussing with reduced scalloping and stable behaviour (Fig. 10).

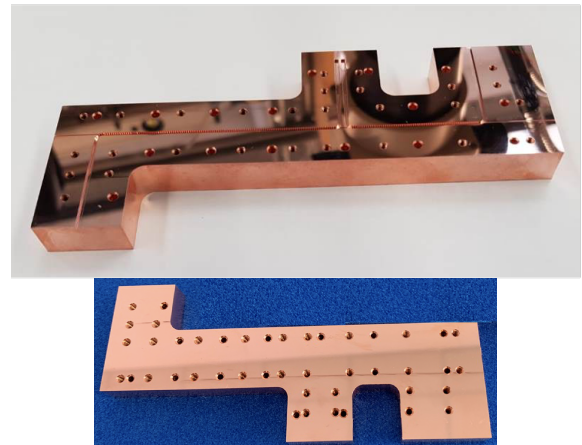


Fig. 11. Two section DCW, top view and lid

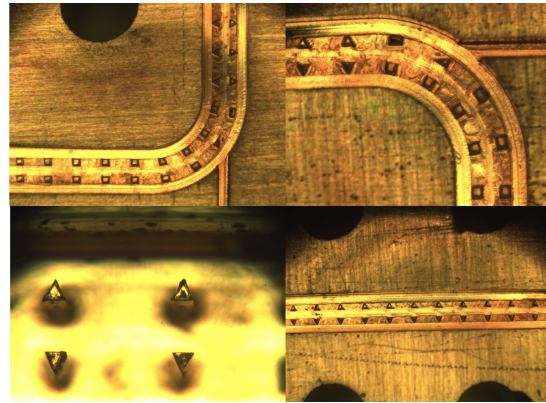


Fig. 12. Details of the D-band DCW and the pillars.

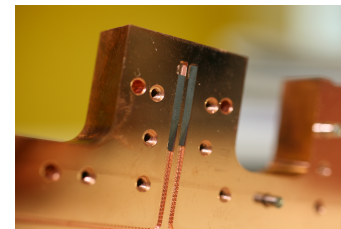


Fig. 13. Detail of the sever with the two graphite absorbers.

### E. Collector

A single stage depressed collector is used to keep simple the fabrication of the first TWT prototype, without a specific requirement for efficiency. The simple design ensures good collection of the spent beam with the backscattering current close to zero. The computed efficiency is about 55 %. The future development is to optimize the depressed collector for efficiency by using 3 or 4 stages.

## III. FABRICATION AND ASSEMBLY OF THE D-BAND TWT

In this section, the fabrication of the parts designed and described in Section II will be discussed.

### A. Double corrugated waveguide

The two-section DCW was fabricated by high precision CNC milling in OFHC copper in two blocks (Primacon CNC

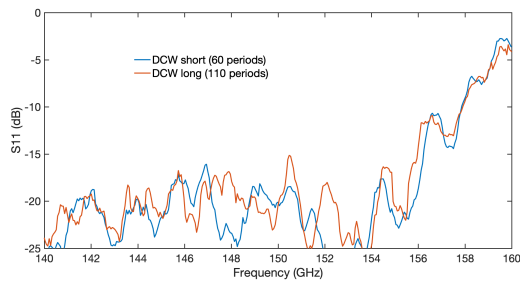


Fig. 14. Measured  $S_{11}$  for the short and long section of the two-section DCW circuit in Fig. 11.

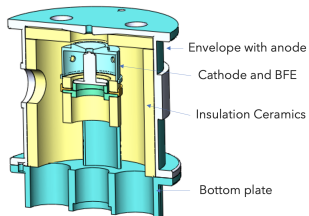


Fig. 15. Cross section of the electron gun.



Fig. 16. Experimental setup gun-collector for electron emission testing.

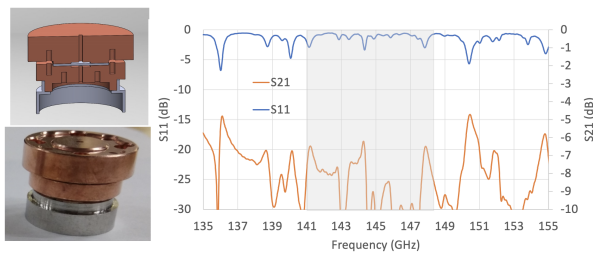


Fig. 17. RF window schematic and fabrication (left), S-parameters (right).

milling). One block (Fig. 11) includes the pillars, the couplers, the sever and the waveguide, the second block is a flat lid (Fig. 11). The advantage of the DCW in comparison to other SWSs used at millimeter waves is that there is no need of alignment of features of the two parts, making the assembly easier. A detail of the sever is shown in Fig. 13. The two idle ports are closed and a graphite wedge placed at the end of the waveguide absorbs the RF signal assuring very low reflection. The details of the pillars are shown in Fig. 12. It is notable the high quality, both for the straight sections and the curved sections. The DCW circuit was measured assembled by screws. The  $S_{11}$  at the output and input ports is shown in Fig. 14. The measured reflection coefficient, below -15 dB in

band, confirms the quality of the manufacturing.

## B. Electron gun

The electron gun together with the SWS is the most expensive part of a TWT. A particular effort has been devoted to the optimisation of the structure and assembly of the electron gun oriented to a low cost production. The electron gun body to support the beam optics has been designed removing the need of multiple brazing of the conventional electron gun structure. It consists of only two metal parts (Fig. 15). One part is the envelope with the anode, the second part is the bottom plate with the support for the cathode subassembly and the aperture for the high voltage feedthroughs. The cathode subassembly includes the dispenser cathode, the beam focussing electrodes and the filament, with a proper isolation and heat shielding. Two ceramic cylinders isolate the high voltage region from the outer envelope. An aperture to connect the vacuum pump is placed on the side of the envelope. The assembly starts with the brazing or laser welding of the feedthroughs at the bottom plate, followed by welding of the heater filament and other terminal to the feedthroughs, and finally the laser welding of the bottom plate to the envelope. The alignment of the bottom plate with the envelope is ensured by the accuracy of the contact surfaces. An iron flange is added externally on the anode side to assemble the electron gun with the DCW circuit and shield the electron gun from the magnetic flux. The first prototype of electron gun has been tested by a gun-collector setup to study the emission and the beam current behaviour (Fig. 16). The transmission achieved is 80% with 6 kV with a peak of 90% at 12.5 kV. This prototype suffered high outgassing during the test, so the full performance could not be achieved. However, the results obtained have confirmed the validity of the design. The final TWT will mount an improved version of the electron gun.

## C. RF Windows

D-band RF windows were designed and realised. The fabricated RF window is shown in Fig. 17. The RF window uses a sheet of Alumina ( $\epsilon_r=9.6$ ) as dielectric. The Alumina is brazed between the two copper waveguide sections. The fabricated RF window and the simulated performance are shown in Fig. 17. It is notable the very wide band of the windows.  $S_{11} \leq -15$  dB over about 20 GHz bandwidth, and  $S_{21} \leq -2$  dB over about 15 GHz, satisfying the frequency band requirements for the TWT. The RF window has a flange to be brazed to the ports of the barrel.

## D. Assembly and machining of the barrel

One of the most delicate phase of the TWT fabrication is the assembly and machining of the barrel including the DCW circuit. The two blocks of the DCW (Fig. 11) are bonded together by diffusion bonding. Diffusion bonding is a process that rebuilds the atomic structure of two separate metal parts at the interface into a single structure when subjected to high pressure and high temperature simultaneously. To increase the difficulty of the process, the bonded structure, in

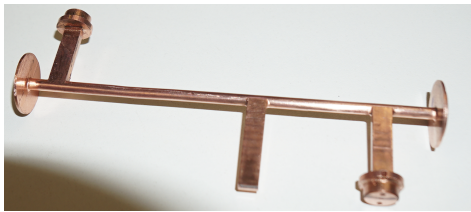


Fig. 18. DCW circuit after CNC machining in form of barrel.

addition to the mechanical robustness, has to be vacuum tight with a vacuum level in the range of  $10^{-9}$  -  $10^{-10}$  torr. The DCW circuit, after bonding, was machined by CNC milling to produce the barrel. Also this process needs high accuracy and machining planning to avoid deformations of the structure that can affect the beam tunnel shape. The barrel has to be perfectly straight along the beam tunnel axis. The diameter of the barrel is defined by the internal diameter of the magnet rings of the ppm system while ensuring metal walls sufficiently thick to maintain the bonding and the vacuum sealing. The fabricated barrel is shown in Fig. 18. To note the input, output and sever branches. The RF flanges are shaped to be brazed with the RF windows. The two flanges at the either ends of the barrels are designed to connect the electron gun and the collector.

#### E. ppm assembly

The vacuum tight barrel permits to assemble the ppm system externally to the barrel by enclosing it with simple cylindrical stainless steel envelope. This envelope is made of several parts to be adapted to the shape of the barrel to which the iron pole pieces are welded to support the magnets. The advantage of this solution is that the envelope does not need to be vacuum tight and the barrel can be built in one piece, simplifying the assembly.

#### F. TWT assembly

The D-band TWT was assembled with the parts described in the previous sections as shown in Fig. 19. The electron gun, the barrel and ppm assembly including the DCW circuit, the RF windows and the collector were not sealed for prototyping purpose, but all the separate assemblies are vacuum tight. The TWT length is about 40 cm including the feedthroughs. The iron pole pieces are assembled along the full length of the DCW to host the magnets. The ceramic isolations in the electron gun and collector permit to keep the body of the TWT at ground potential to be safely manipulated.

A second prototype is in fabrication for the hot testing, with further optimisation of the structure.

### IV. CONCLUSIONS

The design and fabrication of the first D-band TWT based on the double corrugated waveguide has been discussed. Substantial challenges have been addressed with new solutions, such as the triangular pillar to increase the interaction impedance, the fabrication of the DCW circuit in one part for simple assembly, the simple electron gun topology for low cost, the barrel in one piece to reduce the alignment

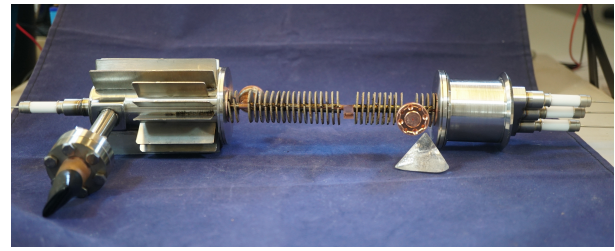


Fig. 19. Full D-band TWT assembly.

difficulties. The fabrication process has demonstrated feasible to build relative low cost TWT suitable for the emerging wireless network market at sub-THz frequencies, to enabling point to multipoint and point to point links with long range and high data rate for future 5G and 6G applications, so far precluded due to lack of adequate transmission power.

### V. ACKNOWLEDGMENT

The authors are grateful to Nicolas Renninson for CNC fabrication support.

### REFERENCES

- [1] S. S. Dhillon and *et al.*, "The 2017 terahertz science and technology roadmap," *Journal of Physics D: Applied Physics*, vol. 50, p. 043001, Jan 2017.
- [2] J. Shi, L. Lv, Q. Ni, H. Pervaiz, and C. Paoloni, "Modeling and analysis of point-to-multipoint millimeter wave backhaul networks," *IEEE Transactions on Wireless Communications*, vol. 18, no. 1, pp. 268–285, 2019.
- [3] C. Paoloni and *et al.*, "Millimeter wave traveling wave tubes for the 21st century," *Journal of Electromagnetic Waves and Applications*, vol. 35, no. 5, pp. 567–603, 2020.
- [4] F. Andre and *et al.*, "Technology, assembly, and test of a w-band traveling wave tube for new 5g high-capacity networks," *IEEE Transactions on Electron Devices*, vol. 67, no. 7, pp. 2919–2924, 2020.
- [5] "Ultrawave website." <http://www.ultrawave2020.eu>, 2017.
- [6] M. Hossain and *et al.*, "D-band transmission hub for point to multipoint wireless distribution," in *2020 50th European Microwave Conference (EuMC)*, pp. 157–160, 2021.
- [7] R. Basu and *et al.*, "On a d-band traveling wave tube for wireless links," in *2020 International Vacuum Electronics Conference (IVEC)*, 2020.
- [8] D. Gamzina and *et al.*, "Nano-cnc machining of sub-thz vacuum electron devices," *IEEE Transactions on Electron Devices*, vol. 63, no. 10, pp. 4067–4073, 2016.
- [9] L. Wenqiang and *et al.*, "Development of d-band continuous-wave folded waveguide traveling-wave tube," in *2015 IEEE International Vacuum Electronics Conference (IVEC)*, 2015.
- [10] M. Field and *et al.*, "Development of a 100-w 200-ghz high bandwidth mm-wave amplifier," *IEEE Transactions on Electron Devices*, vol. 65, no. 6, pp. 2122–2128, 2018.
- [11] Z. Wang and *et al.*, "Development of a 140-ghz folded-waveguide traveling-wave tube in a relatively larger circular electron beam tunnel," *Journal of Electromagnetic Waves and Applications*, vol. 31, no. 17, pp. 1914–1923, 2017.
- [12] K. T. Nguyen and *et al.*, "Design methodology and experimental verification of serpentine/folded-waveguide twts," *IEEE Transactions on Electron Devices*, vol. 61, no. 6, pp. 1679–1686, 2014.
- [13] M. Mineo and C. Paoloni, "Double-corrugated rectangular waveguide slow-wave structure for terahertz vacuum devices," *IEEE Transactions on Electron Devices*, vol. 57, no. 11, pp. 3169–3175, 2010.
- [14] M. Mineo and C. Paoloni, "Improved corrugation cross-sectional shape in terahertz double corrugated waveguide," *IEEE Transactions on Electron Devices*, vol. 59, no. 11, pp. 3116–3119, 2012.
- [15] "Cst studio suite (microwave studio)," 2018.
- [16] C. Paoloni and *et al.*, "Double corrugated waveguide for ka-band traveling wave tube," *IEEE Transactions on Electron Devices*, vol. 62, no. 11, pp. 3851–3856, 2015.